processes

MDPI

Article

Pump-Controlled AGC Micro-Displacement Position Control of Lithium Battery Pole Strip Mill Based on Friction Model

Kai Wang [1], Gexin Chen [1,2,*] and Tiangui Zhang [1]

[1] School of Mechanical Engineering, Yanshan University, Qinhuangdao 066004, China; kaiwang@stumail.ysu.edu.cn (K.W.); tianguiz@stumail.ysu.edu.cn (T.Z.)
[2] Mechanical and Electrical Engineering, Xinjiang Institute of Engineering, Urumqi 830023, China
* Correspondence: jygxchen@ysu.edu.cn; Tel.: +86-0991-7977195

Abstract: Electrode roll-forming refers to rolling a battery electrode into a preset thickness through the electro-hydraulic servo pump-controlled hydraulic roll gap thickness automatic control system (known to as pump-controlled AGC). Compared with the motor servo system, the friction problem of the electro-hydraulic servo system is more serious and the friction problem of the actuator itself is very prominent. Moreover, low-speed performance is one of its core indicators, the friction phenomenon is the most abundant during the low-speed stage and the impact on the servo system is also the most obvious. Therefore, for high-performance electro-hydraulic servo control, friction compensation is not only unavoidable, but also a very difficult problem. Aiming to influence the friction on the position control of the pump-controlled system of a lithium battery pole strip mill, the rolling mechanism and process procedure under micro-displacement position control based on the friction model were studied and compared from the perspective of considering friction factors, and a friction compensation controller based on the LuGre model was designed. The control precision of a pump-controlled AGC system was improved through combination with an adaptive robust controller. Because of the diversity of unmeasurable states of the system, a dual observer was designed, and the known model of the system was added to the observer. In the final comparative experiment, the steady-state accuracy of the friction adaptive robust compensation controller system based on the LuGre model reached ±0.3 μm, which is superior to the fuzzy IMC compensation and traditional PID control strategies.

Keywords: electro-hydraulic servo pump control; friction compensation; LuGre model; position control

Citation: Wang, K.; Chen, G.; Zhang, T. Pump-Controlled AGC Micro-Displacement Position Control of Lithium Battery Pole Strip Mill Based on Friction Model. *Processes* **2023**, *11*, 2587. https://doi.org/10.3390/pr11092587

Academic Editor: Manikandan Palanisamy

Received: 2 August 2023
Revised: 21 August 2023
Accepted: 23 August 2023
Published: 29 August 2023

1. Introduction

Lithium batteries are used as the energy storage power source of electric vehicles, and the safety and driving range of vehicles are closely related to their performance. The production of electrode plates is a crucial component of the lithium–ion battery production process. The quality of the electrode plates directly determines the performance and life of a battery cell. Meanwhile, lithium batteries are among the three core components of electric vehicles [1], and their performance directly determines the vehicle's safety and the endurance mileage of the whole vehicle [2]. The manufacturing and molding of lithium batteries consists of multiple steps, such as mixing, drying, roll compression, slitting, earing, and encapsulation, as shown in Figure 1, and the roll molding of positive and negative electrode plates is one of the key processes and has a great impact on the final performance of the battery. At present, the roll-forming of the lithium battery electrode puts forward high requirements for the control performance of the automatic control of the hydraulic roll gap thickness (AGC) in the hydraulic electrode mill during rolling [3]. Electro-hydraulic servo pump-controlled AGC technology (referred to as pump-controlled AGC) can effectively solve the inherent problems of electro-hydraulic servo valve control technology [4,5], with the advantages of high efficiency, energy savings, a high power/weight ratio, and

environmental friendliness [6,7]. In terms of positioning accuracy, the traditional hydraulic position control system can only guarantee a positioning error of 0.1 mm [8]. Hydraulic control systems are rarely used in micron-level position control systems [9,10]. The uncertainty of the position control process parameters [11–13] and the uncertainty nonlinearity [14–17] of the electro-hydraulic pump control system have become important factors limiting the position control performance.

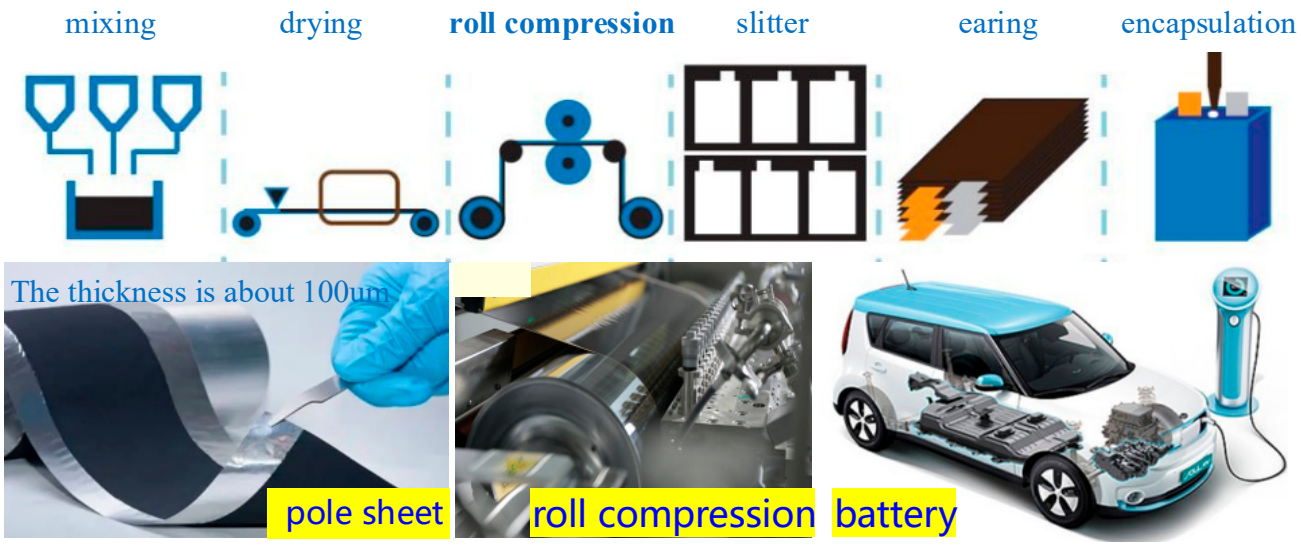

Figure 1. New energy lithium battery manufacturing process.

A good high-performance control strategy is the key for pump-controlled AGC to achieve high-precision rolling of polar sheets [18]. The process requirements of high precision and high response in the rolling process of constant rolling force and constant roll gap pose higher technical challenges to high-performance control. The pump-controlled AGC hydraulic system has problems such as high nonlinearity and strong coupling [19,20], which leads to the thickness deviation of the lithium battery pole sheet after the rolling, which further affects the service performance and safety performance of the lithium battery. In the rolling process, the flow dead zone characteristics, oil compressibility characteristics, and oil leakage characteristics of hydraulic pumps will directly affect the high-precision and high-performance rolling of pump-controlled pole plate mills [21].

Scholars have proposed many solutions to improve the tracking performance [22,23] and position control accuracy [24,25] of nonlinear time-varying control systems. For robust model predictive controller (MPC) technology, Zad et al. [26] adopted a position servo system model to predict the future control effect and improve the position tracking performance. Compared with PID control, this method has significantly improved the control accuracy, robustness, and response speed of the position servo system. Ali et al. [27] and Kim et al. [28] designed a continuous discrete time observer and a nonlinear position-tracking controller with a disturbance observer (DOB) that achieved the goal of improving the target position-tracking performance of EHA systems. For the servo motor pump direct drive system, Bobo et al. [29] designed an ARC controller with backstepping, which adopts an adaptive robust control (ARC) algorithm to accurately track the target trajectory, and has better performance and tracking accuracy compared with the nonlinear flow mapping controller. For the micron-level accurate positioning problem, Peng Xiongbin et al. [30] proposed replacing the servo valve hydraulic system with a servo motor and a displacement amplification hydraulic cylinder, and the position deviation of each hydraulic partition was controlled within 2 μm; the position deviation did not increase with the increase in the rotation angle of the base. Wang Yunfei [31] modeled and analyzed the multi-cylinder cooperative control system of the hydraulic support group and verified

the control method of the pulling and pushing processes of the multi-cylinder cooperative system using the co-simulation model, and the control accuracy was stable within 2 mm.

The above-outlined literature analyzed the position control of the electro-hydraulic servo pump control system theoretically, conducted systematic research and test verification on different controller designs, and expanded the position control and position tracking of the system. However, the test conditions were quite different from the real operating environment of the hydraulic cylinder, and the influence of friction on the position control of the pump control system was not considered or simulated. Friction widely exists in mechanical servo systems, which is one of the main sources of servo system damping and has an important impact on system performance, especially low-speed servo performance [32]. However, at present, there is no research in the literature that has considered friction compensation and combined it with an adaptive, robust controller for an electro-hydraulic servo pump control system. Therefore, this paper focuses on studying the rolling mechanism and process procedure of a pump-controlled AGC system of lithium battery pole plate mills under micro-displacement position control based on the friction model and observes and compares the performance of its position control considering friction factors achieved by different friction models and by designing different controllers. The paper is organized as follows: Section 2 introduces the working principles of a pump-controlled AGC. Section 3 explains the mathematical model of the pump-controlled cylinder system and the friction model and provides details of the equations used in the study. In Section 4, the design of a friction compensation controller based on the LuGre model is presented. Section 5 draws on the performance of the controller. In Section 6, simulation experiments are compared based on the above. In Section 7, on the basis of the above, the practical application experiment of a pump-controlled AGC for lithium battery pole mills is verified. The article is summarized in Section 8.

2. Pump-Controlled AGC Working Principles

As shown in Figures 2 and 3, this paper adopts the scheme of a servo motor with the quantitative pump directly driving and controlling the hydraulic cylinder to form an integrated AGC technology of electro-hydraulic servo pump control, which is composed of the servo motor, quantitative pump, hydraulic cylinder, oil recharge accumulator, functional valve block, etc. In the pump-controlled AGC, there is no key connection between the servo motor and the quantitative pump, and the form of the servo motor's coaxial direct-drive quantitative pump is adopted. The suction and discharge ports of the quantitative pump are directly connected to the two load oil ports of the hydraulic cylinder. The accumulator and check valve are used to store and replenish the oil in the system. The controller outputs control instructions to the servo motor, thereby changing the speed of the quantitative pump to adjust the flow of the system, and thus the output and displacement of the hydraulic cylinder, in order to achieve high-performance control of the system.

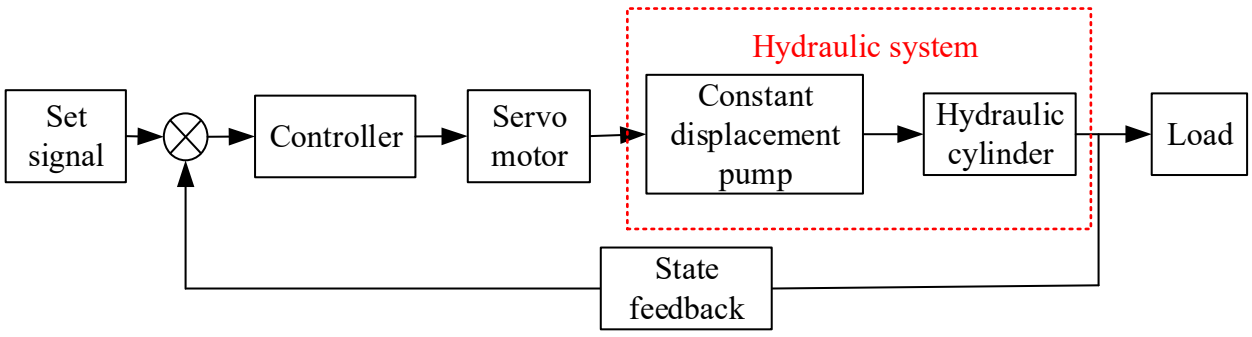

Figure 2. Electrohydraulic servo pump control system working principles frame diagram.

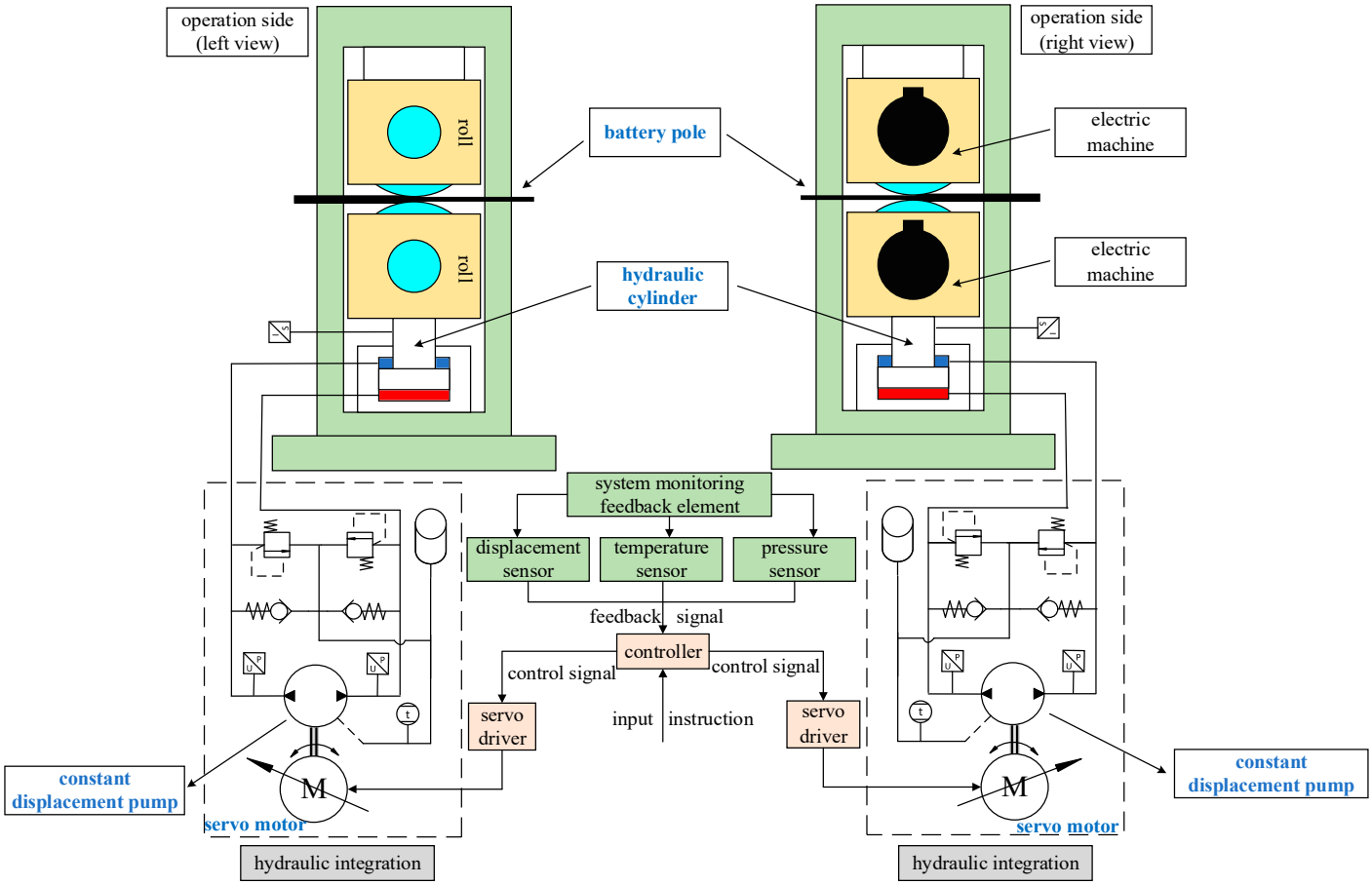

Figure 3. Working principles of the electro-hydraulic servo pump-controlled AGC.

3. Mathematical Model of the Pump-Controlled Cylinder System Based on the Friction Model

3.1. Mathematical Model of the Pump-Controlled System

The flow continuity equation of the double-acting hydraulic cylinder is Laplace transformed and simplified, expressed as:

$$Q_L = A_p X_p s + C_{tc} P_L + V_t P_L s / 4\beta_e \tag{1}$$

where, X_p is the load displacement; A_p is the piston area; C_{ic} and C_{ec} are the internal and external leakage coefficients of the hydraulic cylinder, respectively; C_{tc} is the total leakage coefficient of the hydraulic cylinder, $C_{tc} = C_{ic} + C_{ec}/2$ ($m^3/(s \cdot Pa)$); β_e is the oil elastic stiffness; Q_L is the system flow, $Q_L = (Q_1 + Q_2)/2$ (m^3/s); and Q_1 and Q_2 are the flow into and out of the left chamber of the hydraulic cylinder, respectively.

According to Newton's second law, the balance equation between the output force and the load force of the hydraulic cylinder, and thus the pull transformation, can be obtained as follows:

$$A_p P_L = m_t X_p s^2 + B_p X_p s + K_s X_p + F_L \tag{2}$$

where m is the load quality; B_p is the viscous damping coefficient of oil ($N/(m/s)$); K_s is the spring stiffness; and F_L includes the external load force, friction force, viscous resistance, and another type of resistance that is difficult to model.

3.2. LuGre Friction Model

In order to obtain a linearized system model, the system friction term ignores the nonlinear characteristics of friction during the modeling process. The existence of nonlinear

friction not only creates dead zones but also seriously affects the low-speed performance of the system. When low-speed control is required, the nonlinear characteristics of friction will become a key factor affecting the servo's performance. Therefore, the linear model cannot meet the needs of low-speed servo performance.

The static model can well characterize the macroscopic characteristics of friction but cannot manage the microscopic characteristics of friction, such as pre-slip, variable static friction force, friction memory, etc. In order to describe the macro and micro behaviors of friction more accurately, the LuGre model of dynamic friction was adopted in this paper, describing the friction as:

$$f_m = \sigma_0 z + \sigma_1 \frac{\mathrm{d}z}{\mathrm{d}t} + \sigma_2 \dot{x} \tag{3}$$

where, σ_0, σ_1, and σ_2 represent the main stiffness, damping, and system viscous damping coefficient, respectively. The function $g(\cdot)$, representing static friction behavior, often uses an exponential model, that is:

$$g(\dot{x}) = \alpha_0 + \alpha_1 e^{-(\dot{x}/\dot{x}_s)^\lambda} \tag{4}$$

where $\sigma_0\alpha_0$ and $\sigma_0(\alpha_0 + \alpha_1)$ represent the macroscopic Coulomb friction f_C and the maximum static friction f_s, respectively. $\dot{x} = v(t), \dot{x}_s = v_s$, v_s is the StriBeck speed; σ_0 is the stiffness coefficient; σ_1 is the damping coefficient; and σ_2 is the viscosity coefficient, namely:

$$\sigma_0 g(\dot{x}) = f_C + (f_s - f_C) e^{-(\dot{x}/\dot{x}_s)^\lambda} \tag{5}$$

$$f_m = \sigma_0 z + \sigma_1 \frac{\mathrm{d}z}{\mathrm{d}t} + \sigma_2 \dot{x} = \sigma_0 z + (\sigma_1 + \sigma_2)\dot{x} - \sigma_1 \frac{|\dot{x}|}{\left[f_C + (f_s - f_C) e^{-(\dot{x}/\dot{x}_s)^\lambda}\right]/\sigma_0} z \tag{6}$$

The LuGre model can describe the main behavior of friction. In this paper, an adaptive robust control friction compensation control strategy based on the LuGre friction model was designed to improve the low-speed performance of an electro-hydraulic servo system.

4. Design of Position Controller Based on the LuGre Friction Model

Adaptive control is a control method that can modify its own characteristics to adapt to changes in the dynamic characteristics of objects and loops. Robust control is a control system that can maintain certain performance under certain parameter perturbations. The advantages of the reverse-step method are as follows: (1) the design process of the control function and controller is systematized and structured through reverse design; (2) nonlinear systems with relative order n can be controlled, eliminating the restriction of relative order 1 in classical passive design. Therefore, this paper adopts adaptive robust control combined with the reverse step design method, which combines the respective working mechanisms of adaptive control and robust control and retains their respective advantages, so that the system can still maintain its stability under the conditions of disturbance and unmodeled influencing factors, that is, it has robustness, and at the same time, the control effect is optimized in a certain sense.

Aiming at the existing position control problem of the system, the idea of friction compensation adaptive robust control based on the LuGre model is adopted to design the controller, as shown in Figure 4.

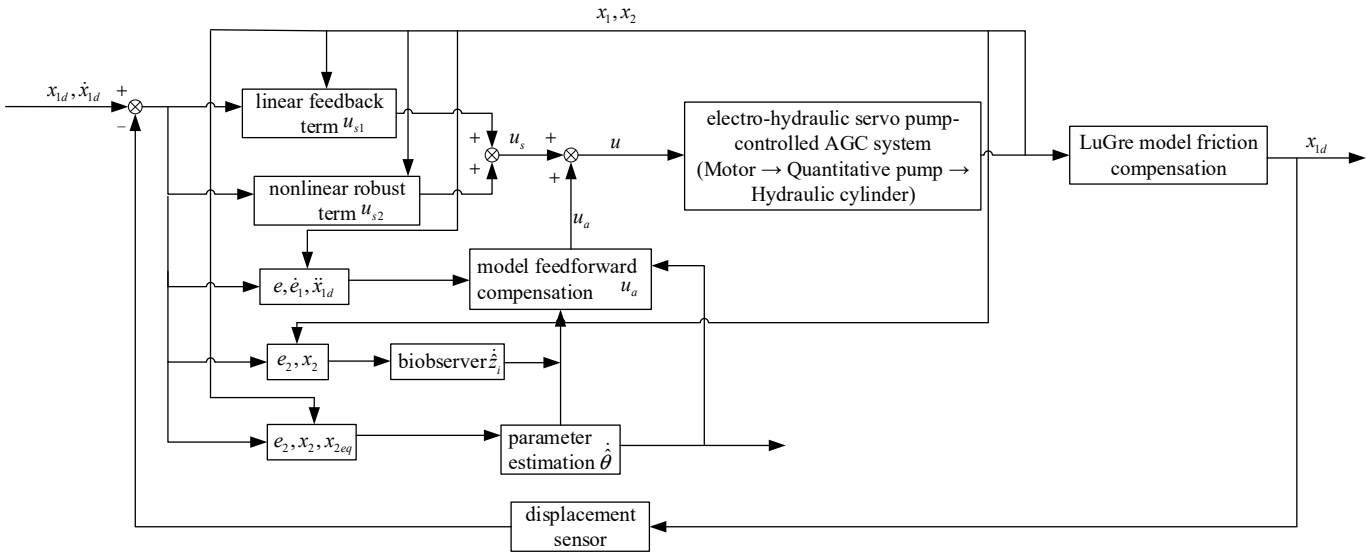

Figure 4. Friction compensation control block diagram.

4.1. System Model and Problem Description

Since the model described by Equation (4) contains nonlinear parameters, for the model-based friction compensation control strategy, it is assumed that the LuGre friction model does not contain unknown nonlinear parameters. Following that, all parameters in friction model (3) are assumed to be linear parameters; hence, a suitable adaptive control strategy can be designed to estimate these unknown friction parameters.

State variables are defined by the LuGre friction model $x = [x_1, x_2, x_3]^{\mathrm{T}} = \left[y, \dot{y}, A(P_1 - P_2)\right]^{\mathrm{T}}$.

$$(P_1 - P_2)A = m\ddot{x}_{\mathrm{p}} + K_{\mathrm{s}}x_{\mathrm{p}} + A_f S_f(\dot{x}_{\mathrm{p}}) + f(x_{\mathrm{p}}, \dot{x}_{\mathrm{p}}, t) \tag{7}$$

Formulas (6) and (7) are combined

$$\begin{aligned} m\dot{x}_2 &= x_3 - K_s x_1 - \sigma_0 z + \sigma_1 \tfrac{|x_2|}{g(x_2)} z - (\sigma_1 + \sigma_2)x_2 - d_n - \widetilde{d}(x_1, x_2, t) \\ &= x_3 - K_s x_1 - \sigma_0 z + \sigma_1 \frac{|\dot{x}|}{\left[f_C + (f_s - f_C)e^{-(\dot{x}/\dot{x}_S)^{\lambda}}\right]/\sigma_0} z - (\sigma_1 + \sigma_2)x_2 - d_n - \widetilde{d}(x_1, x_2, t) \end{aligned} \tag{8}$$

The nonlinear equation of the hydraulic cylinder servo system can be written as:

$$\begin{aligned} &\dot{z} = x_2 - \tfrac{|x_2|}{g(x_2)} z \\ &\dot{x}_1 = x_2 \\ &m\dot{x}_2 = x_3 - K_s x_1 - \sigma_0 z + \sigma_1 \tfrac{|x_2|}{g(x_2)} z - (\sigma_1 + \sigma_2)x_2 - d_n - \widetilde{d}(x_1, x_2, t) \\ &\dot{x}_3 = \tfrac{4An_p}{V_1 + V_2}\beta_e D_p u - \tfrac{4A^2}{V_1 + V_2}\beta_e x_2 - \tfrac{4}{V_1 + V_2}\beta_e C_t x_3 \end{aligned} \tag{9}$$

Combined with Equation (9), the standard form of the nonlinear system corresponding to the state equation of the nonlinear mathematical model of the electro-hydraulic servo system is:

$$\begin{cases} \dot{x} = gu - f \\ y = h(x) = x_3 \end{cases} \tag{10}$$

where, f and g are sufficiently smooth vector fields; y is the system output; and $h(x)$ is the system output function.

The standard form of the nonlinear system corresponding to the nonlinear equation of the hydraulic cylinder servo system can be rewritten as:

$$\begin{pmatrix} \dot{x}_1 \\ \dot{x}_2 \\ \dot{x}_3 \end{pmatrix} = -\begin{pmatrix} f_1 \\ f_2 \\ f_3 \end{pmatrix} + \begin{pmatrix} 0 \\ 0 \\ g_3 \end{pmatrix} u \tag{11}$$

where

$\dot{z} = x_2 - z \cdot |x_2|/g(x_2)$, $f_1 = -x_2$,

$f_2 = (-1/m)\left[x_3 - K_s x_1 - \sigma_0 z + \sigma_1 z \cdot |x_2|/g(x_2) - (\sigma_1 + \sigma_2)x_2 - d_n - \widetilde{d}(x_1, x_2, t)\right]$,

$f_3(x) = 4\beta_e(A^2 x_2 + C_t x_3)/(V_1 + V_2)$, $g_3(x) = 4A\beta_e D_p n_p/(V_1 + V_2) > 0$, $\forall x$.

Additionally, the unknown system parameters are defined as $\theta = [\theta_1, \theta_2, \theta_3, \theta_4]^{\mathrm{T}} = [\sigma_0, \sigma_1, \sigma_1 + \sigma_2, d_n]^{\mathrm{T}}$. Subsequently, the nonlinear equation of the system can be reduced to:

$$\begin{aligned} &\dot{z} = x_2 - z \cdot |x_2|/g(x_2) \\ &\dot{x}_1 = x_2 \\ &m\dot{x}_2 = x_3 - K_s x_1 - \theta_1 z + \theta_2 z \cdot |x_2|/g(x_2) - \theta_3 x_2 - \theta_4 - \widetilde{d}(x_1, x_2, t) \\ &\dot{x}_3 = g_3(x)u - f_3(x) \end{aligned} \tag{12}$$

Hypothesis $\theta \in \Omega_\theta \mathrm{def}\{\theta : \theta_{\min} \le \theta \le \theta_{\max}\}$, $\left|\widetilde{d}(x_1, x_2, t)\right| \le \delta_d(x_1, x_2, t)$, where $\theta_{\max} = [\theta_{1\max}, \cdots, \theta_{4\max}]^{\mathrm{T}}$ and $\theta_{\min} = [\theta_{1\min}, \cdots, \theta_{4\min}]^{\mathrm{T}}$ are the upper and lower boundaries of vector θ; δ_d is a known function.

Facing the difficulty of designing the friction compensation controller based on the LuGre model, the design target of the system controller is given the system reference signal $y_d(t) = x_{1d}(t)$. A bounded control input u is designed for the system output tracks, with the reference signal $y = x_1$ as much as possible. The control input u is divided into two parts, namely u_a and u_s, and u_a is the model compensation item, similar to an adaptive controller based on a system model, and the parameter estimates are updated in real time by an online adaptive process. u_s is also divided into two parts: u_{s1} and u_{s2}, where u_{s1} can be regarded as the linear, stable feedback of the system. The reference signal $x_{1d}(t)$ is assumed to be third-order continuous, and the system expects position instructions, speed instructions, acceleration instructions, and acceleration instructions to be bounded.

4.2. Design of the Adaptive Robust Friction Compensation Controller Based on the LuGre Model

4.2.1. Robust Controller Design

Since system equations have mismatched parameter uncertainties, the inverse design method must be used.

Step 1: From system Equation (12), the following error variables are defined:

$$\begin{aligned} &e_1 = x_1 - x_{1d} \\ &e_2 = \dot{e}_1 + k_1 e_1 = x_2 - x_{2eq}, x_{2eq} \mathrm{def} \dot{x}_{1d} - k_1 e_1 \end{aligned} \tag{13}$$

where k_1 is the positive feedback gain.

The main design goal is to make e_2 approach 0, the dual-observer structure is used to estimate the different characteristics of the state z and the mapping function is used to ensure that the estimation of the observer is controlled.

The upper and lower bounds of different estimates, z_1 and z_2, for each given state z are $z_{1\max} = z_{2\max} = z_{\max} = \alpha_0 + \alpha_1$, $z_{1\min} = z_{2\min} = z_{\min} = -(\alpha_0 + \alpha_1)$.

For the unknown parameter θ, the following parameter adaptive law is defined:

$$\dot{\hat{\theta}} = \mathrm{Proj}_{\hat{\theta}}(\Gamma\tau) = \begin{cases} 0, & \hat{\theta} = \theta_{\max} \text{ and } \Gamma\tau > 0 \\ 0, & \hat{\theta} = \theta_{\min} \text{ and } \Gamma\tau < 0 \\ \Gamma\tau, & \text{else} \end{cases}, \theta_{\min} \le \hat{\theta}(0) \le \theta_{\max} \tag{14}$$

where $\widetilde{\theta} = \hat{\theta} - \theta$, $\boldsymbol{\Gamma} > 0$ represents the adaptive gain and τ is the parametric adaptive function.

From Equation (13), we can see that:

$$m\dot{e}_2 = m\dot{x}_2 - m\dot{x}_{2eq} = x_3 - \theta_1 z + \theta_2 \frac{|x_2|}{g(x_2)} z - \theta_3 x_2 - \theta_4 - m\dot{x}_{2eq} - K_s x_1 - \widetilde{d}(x_1, x_2, t) \tag{15}$$

$k_{2s1} > 0$ is the controller design parameter, and the integrated design feedback gain k_1 and k_{2s1} are large enough to make Λ_2, as defined below a positive definite matrix. The deviation between the control function α_2 and the virtual control input x_3 is defined as $e_3 = x_3 - \alpha_2$.

$$\Lambda_2 = \begin{bmatrix} k_1^3 & -k_1^3/2; & -k_1^3/2 & k_{2s1} \end{bmatrix} \tag{16}$$

According to Formula (16), α_{2s2} can be designed to satisfy the following stabilization conditions:

$$e_2 \left\{ \alpha_{2s2} - \varphi_2^{\mathrm{T}} \widetilde{\theta} + \theta_1 \widetilde{z}_1 - \theta_2 \widetilde{z}_2 \cdot |x_2|/g(x_2) - K_s x_1 - \widetilde{d}(x_1, x_2, t) \right\} \leq \varepsilon_2 \tag{17}$$

$$e_2 \alpha_{2s2} \leq 0 \tag{18}$$

where ε_2 is an arbitrarily small positive controller design parameter. As can be seen from Equation (17), the designed α_{2s2} is a robust controller.

4.2.2. Design of the Adaptive Robust Controller

The Lyapunov function is defined as follows:

$$V_2 = me_2^2/2 + k_1^2 e_1^2/2 \tag{19}$$

Its time derivative is:

$$\begin{aligned} \dot{V}_2 &= m\dot{e}_2 e_2 + k_1^2 e_1 \dot{e}_1 \\ &= e_2 e_3 - k_1^2 e_1^2 + k_1^2 e_1 e_2 - k_{2s1} e_2^2 \\ &+ e_2 \left[\alpha_{2s2} - \varphi_2^{\mathrm{T}} \widetilde{\theta} + \theta_1 \widetilde{z}_1 - \theta_2 \widetilde{z}_2 \cdot |x_2|/g(x_2) - K_s x_1 - \widetilde{d}(x_1, x_2, t) \right] \end{aligned} \tag{20}$$

Step 2: From the third equation of the system and according to the definition of e_3, we can see that: $\dot{e}_3 = g_3 u - f_3 - \dot{\alpha}_2$, where

$$\begin{aligned} &\dot{\alpha}_2 = \dot{\alpha}_{2c} - \dot{\alpha}_{2u} \\ &\dot{\alpha}_{2c} = \tfrac{\partial \alpha_2}{\partial t} + \tfrac{\partial \alpha_2}{\partial x_1} x_2 + \tfrac{\partial \alpha_2}{\partial x_2} \hat{x}_2 + \tfrac{\partial \alpha_2}{\partial \hat{\theta}} \dot{\hat{\theta}} + \tfrac{\partial \alpha_2}{\partial \hat{z}_1} \dot{\hat{z}}_1 + \tfrac{\partial \alpha_2}{\partial \hat{z}_2} \dot{\hat{z}}_2 \\ &\dot{\alpha}_{2u} = \tfrac{\partial \alpha_2}{\partial x_2} \widetilde{\dot{x}}_2 \end{aligned} \tag{21}$$

where, with $\dot{\alpha}_{2c}$ as the computable partial differential part, which is used for the design of the actual controller u; $\dot{\alpha}_{2u}$ is the incomputable part, and a robust controller is designed to stabilize this uncertainty. The limits of the partial derivative of α_2 at $x_2 = 0$ are bounded.

The design of the adaptive robust controller u has the following structure, where $k_{3s1} > 0$ is the design parameter of the controller:

$$\begin{aligned} &u = u_a + u_s \\ &u_a = (f_3 + \dot{\alpha}_{2c})/g_3 \\ &u_s = (u_{s1} + u_{s2})/g_3 \\ &u_{s1} = -k_{3s1} e_3 \end{aligned} \tag{22}$$

$\varphi_3^{\mathrm{T}}\mathrm{def} - \frac{1}{m}\frac{\partial \alpha_2}{\partial x_2}\varphi_2^{\mathrm{T}}$ is defined and controller (22) is substituted into $\dot{e}_3$

$$\begin{aligned}\dot{e}_3 &= -k_{3s1}e_3 + u_{s2} - \varphi_3^{\mathrm{T}}\widetilde{\theta} - \frac{1}{m}\frac{\partial \alpha_2}{\partial x_2}\theta_1\widetilde{z}_1 \\ &+ \frac{1}{m}\frac{\partial \alpha_2}{\partial x_2}\theta_2\frac{|x_2|}{g(x_2)}\widetilde{z}_2 + \frac{1}{m}\frac{\partial \alpha_2}{\partial x_2}K_s x_1 + \frac{1}{m}\frac{\partial \alpha_2}{\partial x_2}\widetilde{d}(x_1, x_2, t)\end{aligned} \tag{23}$$

According to Formula (23), u_{s2} can be designed to satisfy the following stabilization conditions:

$$e_3\left\{u_{s2} - \varphi_3^{\mathrm{T}}\widetilde{\theta} - \frac{1}{m}\frac{\partial \alpha_2}{\partial x_2}\theta_1\widetilde{z}_1 + \frac{1}{m}\frac{\partial \alpha_2}{\partial x_2}\theta_2\frac{|x_2|}{g(x_2)}\widetilde{z}_2 + \frac{1}{m}\frac{\partial \alpha_2}{\partial x_2}K_s x_1 + \frac{1}{m}\frac{\partial \alpha_2}{\partial x_2}\widetilde{d}(x_1, x_2, t)\right\} \le \varepsilon_3 \tag{24}$$

$$e_3 u_{s2} \le 0 \tag{25}$$

where ε_3 is a controller design parameter that can be arbitrarily small and positive, and u_{s2} is a robust controller.

As can be seen from Formula (24), the designed u_{s2} is a robust controller, which is used to govern various uncertainties of the system model, namely, parameter uncertainties $\widetilde{\theta}$ and $\widetilde{d}$. Equation (25) shows that u_{s2} is naturally dissipative, that is, as the control error e_3 decreases, its control quantity also decreases, which minimizes the coupling between the robust controller and the adaptive control law so that the functions between them do not overlap as much as possible.

5. Performance of the Adaptive Robust Controller

In the controller design outlined in Section 4.2.1, dual observers are used to estimate the different characteristics of state z, while mapping functions are used to ensure that the estimation of the observers is controlled, and ι_i is the adjustment function of the observer z_i, respectively.

$$\dot{\hat{z}}_i = \mathrm{Proj}_{\hat{z}_i}(\iota_i), \quad z_{\min} \le z_i(0) \le z_{\max} \tag{26}$$

Theorem 1. *Using the adaptive law of discontinuous mapping (14) and setting $\tau = \varphi_2 e_2 + \varphi_3 e_3$, $\gamma_i > 0$is the gain of the observer, and the adjustment function of the observer in Equation (26) is defined as:*

$$\iota_i = x_2 - \frac{|x_2|}{g(x_2)}\hat{z}_i - \gamma_i\left(e_2 - \frac{1}{m}\frac{\partial \alpha_2}{\partial x_2}e_3\right) \tag{27}$$

For any adaptive function τ, the adjustment function of the observer ι_i, the discontinuous mapping (14) has the following properties:

$$\begin{aligned}&\widetilde{\theta}^{\mathrm{T}}\left[\Gamma^{-1}\dot{\hat{\theta}} - \tau\right] \le 0, \forall\tau \\ &\widetilde{z}_i\left\{\dot{\hat{z}}_i - \iota_i\right\} \le 0\end{aligned} \tag{28}$$

5.1. Performance Conclusion of the Adaptive Robust Controller A

All signals in a closed-loop controller are bounded, and the Lyapunov function is defined as follows:

$$V_3 = V_2 + \frac{1}{2}e_3^2 \le \exp(-\mu t)V_3(0) + \frac{\varepsilon}{\mu}[1 - \exp(-\mu t)] \tag{29}$$

where $\mu = 2\lambda_{\min}(\Lambda_3)\min\{1/k_1^2, 1/m, 1\}$, $\lambda_{\min}(\Lambda_3)$ is the smallest eigenvalue of Λ_3, $\varepsilon = \varepsilon_2 + \varepsilon_3$.

Matrix Λ_3 is defined as a positive definite matrix (comprehensive design feedback gain k_1, k_{2s1}, k_{3s1} is large enough):

$$\Lambda_3 = \begin{bmatrix} k_1^3 & -k_1^3/2 & 0; & -k_1^3/2 & k_{2s1} & -1/2; & 0 & -1/2 & k_{3s1} \end{bmatrix} \tag{30}$$

5.2. Conclusion of the Adaptive Robust Controller Performance B

Under certain times, t_0, there is only parametric uncertainty in the system. In addition to conclusion A, controller (29) can also obtain asymptotic tracking performance: that is, when $t \to \infty, e \to 0$, where e is defined as $e = [e_1, e_2, e_3]^{\mathrm{T}}$.

5.3. Proof of Conclusion

The time derivative of V_3 is:

$$\dot{V}_3 = \dot{V}_2 + e_3\dot{e}_3 \le e_2e_3 - k_1^2e_1^2 + k_1^2e_1e_2 - k_{2s1}e_2^2 - k_{3s1}e_3^2 + \varepsilon_2 + \varepsilon_3 \tag{31}$$

This is known according to condition (30)

$$\dot{V}_3 \le -e^{\mathrm{T}}\Lambda_3 e + \varepsilon \le -\lambda_{\min}(\Lambda_3)\left(e_1^2 + e_2^2 + e_3^2\right) + \varepsilon \le \varepsilon - \mu V_3 \tag{32}$$

According to the contrast principle $V_3 \le \exp(-\mu t)V_3(0) + (\varepsilon/\mu)[1 - \exp(-\mu t)]$, V_3 is globally bounded, that is, e_1, e_2, and e_3 are bounded by the position, speed, and acceleration instructions of the system, and the estimation of unknown parameters and state z. Thus, it can be easily deduced that all signals of the closed-loop system are bounded. Conclusion A is then proven. When considering conclusion B below, since there is only parameter uncertainty in the system at this time, the Lyapunov function is defined as follows:

$$V_s = V_3 + \widetilde{\theta}^{\mathrm{T}}\Gamma^{-1}\widetilde{\theta}/2 + \gamma_1^{-1}\theta_1\widetilde{z}_1^2/2 + \gamma_2^{-1}\theta_2\widetilde{z}_2^2/2 \tag{33}$$

It is known from Equations (20) and (23) that its time differential is

$$\begin{aligned} \dot{V}_s &= \dot{V}_3 + \widetilde{\theta}^{\mathrm{T}}\Gamma^{-1}\dot{\hat{\theta}} + \gamma_1^{-1}\theta_1\widetilde{z}_1\dot{\widetilde{z}}_1 + \gamma_2^{-1}\theta_2\widetilde{z}_2\dot{\widetilde{z}}_2 \\ &= e_2e_3 - k_1^3e_1^2 + k_1^2e_1e_2 - k_{2s1}e_2^2 - k_{3s1}e_3^2 + e_2\left[\alpha_{2s2} - \varphi_2^{\mathrm{T}}\widetilde{\theta} + \theta_1\widetilde{z}_1 - \theta_2\tfrac{|x_2|}{g(x_2)}\widetilde{z}_2 - K_sx_1 - \widetilde{d}(x_1, x_2, t)\right] \\ &+ e_3\left[-k_{3s1}e_3 + u_{s2} + \tfrac{1}{m}\tfrac{\partial\alpha_2}{\partial x_2}\varphi_2^{\mathrm{T}}\widetilde{\theta} - \tfrac{1}{m}\tfrac{\partial\alpha_2}{\partial x_2}\theta_1\widetilde{z}_1 + \tfrac{1}{m}\tfrac{\partial\alpha_2}{\partial x_2}\theta_2\tfrac{|x_2|}{g(x_2)}\widetilde{z}_2 + \tfrac{1}{m}\tfrac{\partial\alpha_2}{\partial x_2}K_sx_1 + \tfrac{1}{m}\tfrac{\partial\alpha_2}{\partial x_2}\widetilde{d}(x_1, x_2, t)\right] \\ &+ \widetilde{\theta}^{\mathrm{T}}\Gamma^{-1}\dot{\hat{\theta}} + \gamma_1^{-1}\theta_1\widetilde{z}_1\dot{\widetilde{z}}_1 + \gamma_2^{-1}\theta_2\widetilde{z}_2\dot{\widetilde{z}}_2 \end{aligned} \tag{34}$$

Obtained by conditions (18) and (25)

$$\begin{aligned} \dot{V}_s \le\ & -\lambda_{\min}(\Lambda_3)\left(e_1^2 + e_2^2 + e_3^2\right) + \widetilde{\theta}^{\mathrm{T}}\Gamma^{-1}\dot{\hat{\theta}} - \varphi_2^{\mathrm{T}}\widetilde{\theta}e_2 - \varphi_3^{\mathrm{T}}\widetilde{\theta}e_3 \\ & + \theta_1\widetilde{z}_1\left\{\gamma_1^{-1}\dot{\hat{z}}_1 - \gamma_1^{-1}\left[x_2 - \tfrac{|x_2|}{g(x_2)}(\hat{z}_1 - \widetilde{z}_1)\right] + e_2 - e_3\tfrac{1}{m}\tfrac{\partial\alpha_2}{\partial x_2}\right\} \\ & + \theta_2\widetilde{z}_2\left\{\gamma_2^{-1}\dot{\hat{z}}_2 - \gamma_2^{-1}\left[x_2 - \tfrac{|x_2|}{g(x_2)}(\hat{z}_2 - \widetilde{z}_2)\right] - \tfrac{|x_2|}{g(x_2)}e_2 + \tfrac{1}{m}\tfrac{\partial\alpha_2}{\partial x_2}\tfrac{|x_2|}{g(x_2)}e_3\right\} \end{aligned} \tag{35}$$

From the definition of the adaptive law (14) and τ, the definition of the state observer (26) and the definition of the regulating function ι_i are known as:

$$\begin{aligned} \dot{V}_s \le\ & -\lambda_{\min}(\Lambda_3)\left(e_1^2 + e_2^2 + e_3^2\right) - \gamma_1^{-1}\tfrac{|x_2|}{g(x_2)}\theta_1\widetilde{z}_1^2 - \gamma_2^{-1}\tfrac{|x_2|}{g(x_2)}\theta_2\widetilde{z}_2^2 + \widetilde{\theta}^{\mathrm{T}}\left[\Gamma^{-1}\dot{\hat{\theta}} - \tau\right] \\ & + \theta_1\widetilde{z}_1\left\{\gamma_1^{-1}\left[\dot{\hat{z}}_1 - \iota_1\right]\right\} + \theta_2\widetilde{z}_2\left\{\gamma_2^{-1}\left[\dot{\hat{z}}_2 - \iota_2\right]\right\} \end{aligned} \tag{36}$$

According to (28):

$$\dot{V}_s \le -\lambda_{\min}(\Lambda_3)\left(e_1^2 + e_2^2 + e_3^2\right) - \gamma_1^{-1}\theta_1\widetilde{z}_1^2 \cdot |x_2|/g(x_2) - \gamma_2^{-1}\theta_2\widetilde{z}_2^2 \cdot |x_2|/g(x_2) \tag{37}$$

Therefore, $V_s < V_s(0)$ and $e, \widetilde{\theta}, \widetilde{z}_1, \widetilde{z}_2 \in L_\infty, e \in L_2$, and from Equations (13), (15) and (23), we can see that $\dot{e} \in L_\infty$; therefore, e is uniformly continuous, and when $t \to \infty$, $e \to 0$, thus proving conclusion B.

6. Simulation Verification

This section examines the performance of the designed controller. For Stribeck speed $x_{2s} = 0.01$ m/s, as shown in Figure 5, the system low-speed instruction $x_{1d} = 0.002\sin(2t)\left[1 - \exp\left(-0.01t^3\right)\right]$ is provided. ARCm, a friction adaptive robust compensation controller based on the LuGre model, is proposed in this section. The traditional PID controller is based on a simple approximate friction model, which only compensates for the viscous friction and part of the Coulomb friction. The ARCm control strategy proposed in this paper accurately contains the structure information of the system friction, so the tracking error, adaptive effect, friction identification, and parameter estimation are much better than the PID control strategy, which only approximates part of the friction structure.

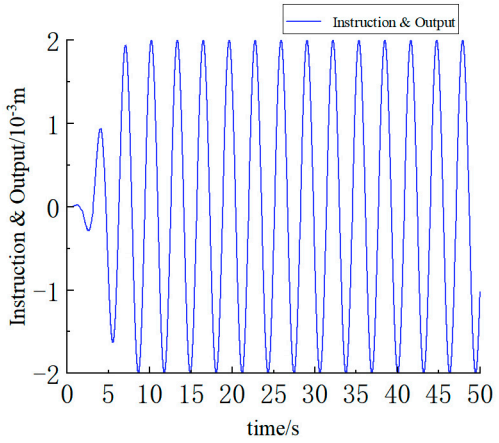

Figure 5. System low−speed instruction.

According to the analysis in Figure 6, the friction adaptive robust compensation controller based on the LuGre model designed and proposed in this paper shows relatively good control performance in terms of system dynamic response and steady-state control, has a good position-following process, a small system position overshoot, and a small steady-state error, and the time to stabilize is about 2 s. However, at this time, other control methods are still fluctuating up and down and have not become stable.

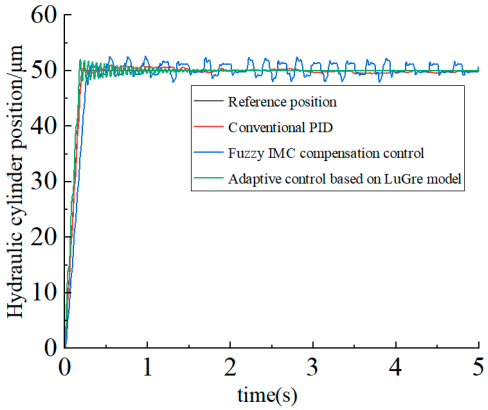

Figure 6. Displacement process diagram of the hydraulic cylinder piston.

The analysis in Figure 7 shows that the steady-state accuracy of the system can reach ±0.3 μm using the friction adaptive robust compensation controller based on the LuGre

model, and become stable when the time is about 2 s, while the steady-state accuracy can reach ±0.7 μm using the fuzzy IMC compensation control strategy. The steady-state accuracy of the system using the traditional PID control strategy can only reach ±2.5 μm, which has a large steady-state error. The results show that the friction adaptive robust compensation control strategy based on the LuGre model can obviously improve the control precision of the pump-controlled AGC system position control.

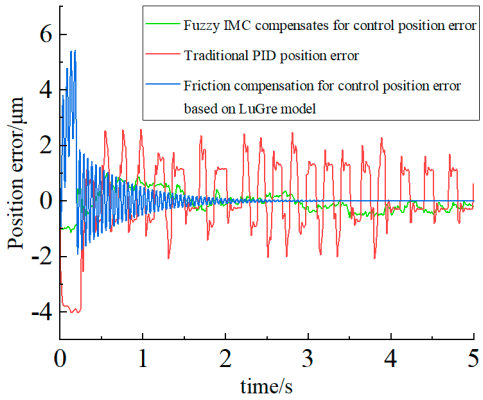

Figure 7. Output position error diagram of the hydraulic cylinder.

7. Practical Application of Micro-Displacement Control in the Pump-Controlled AGC System of a Lithium Battery Pole Strip Mill

In order to verify the precise performance of the micro-displacement control of the lithium battery pole strip mill pump-controlled AGC system, control tests were carried out on the pump-controlled AGC of the lithium battery pole strip mill. The equipment platform is shown in Figure 8. The reliability of the friction adaptive robust compensation controller based on the LuGre model was verified by comparing the traditional PID controller with the roller-forming experiment of the negative electrode plates of the lithium battery.

Given the "S"-type slope track signals resulting from 100 μm from 82.06 mm to 82.16 mm, 50 μm from 82.06 mm to 82.11 mm, and 10 μm from 82.06 mm to 82.07 mm, respectively, the system displacement and error curves are shown in Figures 9 and 10.

Through experimental research and comparative analysis, the following results were obtained: the adjustment of traditional PID control under different working conditions has a certain degree of gapping, and the steady-state accuracy of the system is poor, only reaching ±8 μm with 100 μm and 50 μm displacements and ±6 μm with a 10 μm displacement. The friction adaptive robust compensation control based on the LuGre model has a small overshoot before reaching a steady state; its steady-state control accuracy can reach ±2 μm, and the time to reach the steady state is 1–2 s faster than that of a traditional PID control. Therefore, according to the above experimental results, it can be determined that the position control accuracy of a pump-controlled AGC control system can be significantly improved by adopting the friction adaptive robust compensation control strategy based on the LuGre model, as proposed in this paper.

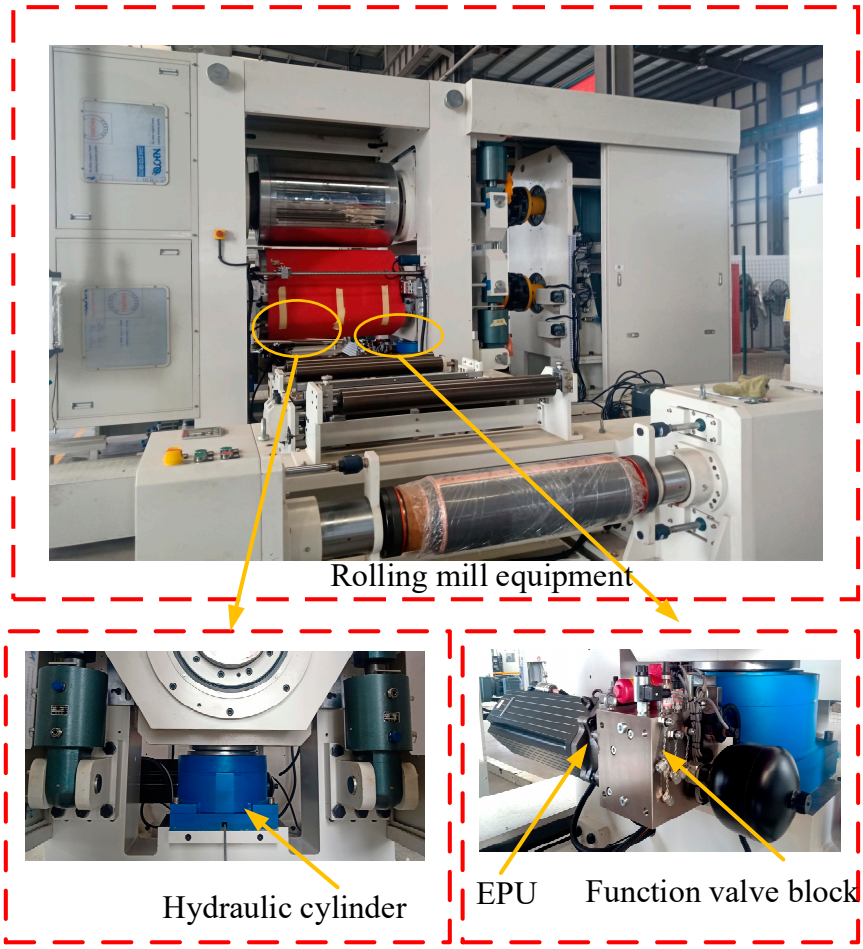

Figure 8. Pump-controlled AGC equipment diagram.

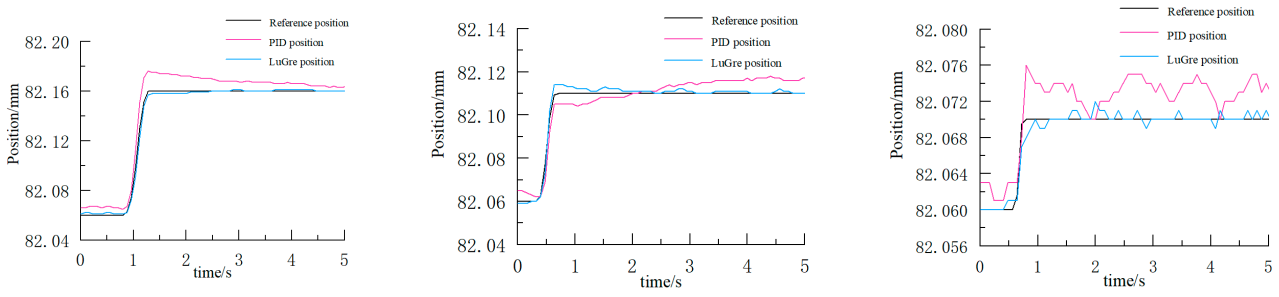

Figure 9. Position curves of the pump-controlled AGC system of a pole plate mill. (**a**) Displacement: 100 μm. (**b**) Displacement: 50 μm. (**c**) Displacement: 10 μm.

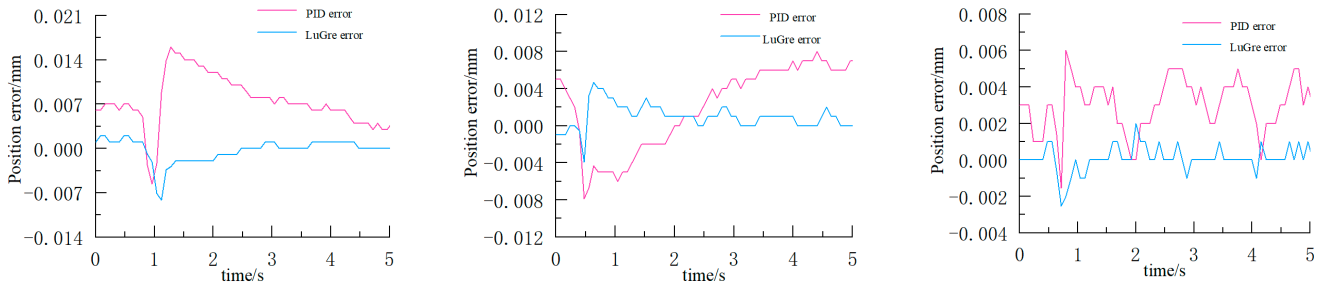

Figure 10. Error curve of the pump−controlled AGC system of a pole plate mill. (**a**) Displacement error: 100 μm. (**b**) Displacement error: 50 μm. (**c**) Displacement error: 10 μm.

8. Conclusions

Friction is one of the main sources of servo system damping and has important effects on system performance, especially low-speed servo performance. During the low-speed stage of the electro-hydraulic servo system, the friction phenomenon is the most abundant, and its influence on the servo system is also the most obvious. Therefore, for high-performance electro-hydraulic servo control, friction compensation is an unavoidable and very difficult problem. In order to improve the position control performance of the system, an adaptive, robust controller with excellent performance was designed based on the dynamic friction model. The adaptive robust controller was combined with the friction model to solve the low-speed servo demands of the system. The friction adaptive robust compensation controller, fuzzy IMC compensation controller, and traditional PID controller based on the LuGre model were designed and built based on the pump control system simulation platform. Comparing the simulation results of the three controllers, it was proven that the friction adaptive robust compensation control strategy based on the LuGre model has better steady-state accuracy and response speed. The experimental results show that the friction adaptive robust compensation control strategy based on the LuGre model proposed in this paper can effectively improve the position control accuracy of the pump-controlled AGC system.

However, the LuGre model also contains discontinuous functions, which often make it difficult to realize the final control law for systems such as electro-hydraulic servo systems that need to deal with uncertainty by means of inversion design, because the solution of the final control law must manage the derivation of the discontinuous function.

Author Contributions: Funding acquisition, G.C.; formal analysis, K.W.; methodology, G.C. and K.W.; project administration, T.Z.; resources, G.C. and K.W.; software, K.W.; writing—original draft, K.W.; writing—review and editing, K.W. and G.C.; supervision, K.W. and G.C. All authors have read and agreed to the published version of the manuscript.

Funding: This research was funded by the National Natural Science Foundation of China (Grant No. 52275066), the Science and Technology Research Project of Colleges and Universities of Hebei Province (ZD2021340).

Institutional Review Board Statement: Not applicable.

Informed Consent Statement: Not applicable.

Data Availability Statement: Not applicable.

Conflicts of Interest: The authors declare no conflict of interest.

References

1. Hong, J.; Ma, F.; Xu, X.; Yang, J.; Zhang, H. A novel mechanical-electric-hydraulic power coupling electric vehicle considering different electrohydraulic distribution ratios. *Energy Convers. Manag.* **2021**, *249*, 114870. [CrossRef]
2. Ren, D.; Lu, L.; Shen, P.; Feng, X.; Han, X.; Ouyang, M. Battery remaining discharge energy estimation based on prediction of future operating conditions. *J. Energy Storage* **2019**, *25*, 100836. [CrossRef]
3. Xiao, Y.; Deng, S.; Liu, W.; Zhou, W.; Wan, F. Optimized Design of Battery Pole Control System Based on Dual-chip Architecture. *PLoS ONE* **2022**, *17*, e0264285. [CrossRef]
4. Sun, J.; Xiang, W.; Huang, H.; Yuan, Z.; Li, J. Research progress of electrode plate rolling technology for lithium battery. *China Metall.* **2021**, *31*, 12–18.
5. Deng, W.; Yao, J.; Wang, Y.; Yang, X.; Chen, J. Output feedback backstepping control of hydraulic actuators with valve dynamics compensation. *Mech. Syst. Signal Process.* **2021**, *158*, 107769. [CrossRef]
6. Yang, M.; Yan, G.; Zhang, Y.; Zhang, T.; Ai, C. Research on high efficiency and high dynamic optimal matching of the electro-hydraulic servo pump control system based on NSGA-II. *Heliyon* **2023**, *9*, e13805. [CrossRef] [PubMed]
7. Wang, W.; Du, W.; Cheng, C.; Lu, X.; Zou, W. Output feedback control for energy-saving asymmetric hydraulic servo system based on desired compensation approach. *Appl. Math. Model.* **2022**, *101*, 360–379. [CrossRef]
8. Wang, C.; Zhang, Z.; Wang, H.; Zhao, B.; Quan, L. Disturbance observer-based output feedback control of hydraulic servo system considering mismatched uncertainties and internal pressure dynamics stability. *IET Control Theory Appl.* **2020**, *14*, 1046–1056. [CrossRef]
9. Xu, Y.X.; Niu, L.C.; Yang, H.; Xiao, Y.C.; Xiao, Y.J. Optimization of Lithium Battery Pole Piece Thickness Control System Based on GA-BP Neural Network. *J. Nanoelectron. Optoelectron.* **2019**, *14*, 978–986. [CrossRef]
10. Jiang, W.; Jia, P.; Yan, G.; Chen, G.; Ai, C.; Zhang, T.; Liu, K.; Jia, C.; Shen, W. Dynamic response analysis of control loops in an electro-hydraulic servo pump control system. *Processes* **2022**, *10*, 1647–1666. [CrossRef]
11. Fu, Y.L.; Han, X.; Yang, R.; Qi, H.T.; Fu, J. Review on design methods of electro-hydrostatic actuator. *J. Beijing Univ. Aeronaut. Astronsutics* **2017**, *43*, 1939–1952.
12. Guo, Q.; Zhang, Y.; Celler, B.G.; Su, S.W. State-Constrained Control of Single-Rod Electrohydraulic Actuator with Parametric Uncertainty and Load Disturbance. *IEEE Trans. Control. Syst. Technol.* **2017**, *26*, 2242–2249. [CrossRef]
13. Guo, Q.; Yin, J.; Yu, T.; Jiang, D. Saturated Adaptive Control of Electrohydraulic Actuator with Parametric Uncertainty and Load Disturbance. *IEEE Trans. Ind. Electron.* **2017**, *64*, 7930–7941. [CrossRef]
14. Huang, P.; Gu, Y.; Li, H.; Mohammad, Y.; Qiu, G. An Optimal Tolerance Design Approach of Robot Manipulators for Positioning Accuracy Reliability. *Reliab. Eng. Syst.Saf.* **2023**, *237*, 109347. [CrossRef]
15. Zhang, Q.; Wei, J.; Fang, J.; Li, M. Nonlinear Motion Control of the Hydraulic Press Based on an Extended Piecewise Disturbance Observer. *Proc. Inst. Mech. Eng. Part I J. Syst. Control. Eng.* **2016**, *230*, 830–850. [CrossRef]
16. Wang, C.; Quan, L.; Jiao, Z.; Zhang, S. Nonlinear Adaptive Control of Hydraulic System with Observing and Compensating Mismatching Uncertainties. *IEEE Trans. Control. Syst. Technol.* **2017**, *26*, 927–938. [CrossRef]
17. Zheng, Y.; Sun, R.; Li, F.; Liu, Y.; Song, R.; Li, Y. Parameter identification and position control for helical hydraulic rotary actuators based on particle swarm optimization. *Mechatronics* **2023**, *94*, 103006. [CrossRef]
18. Li, Y.; Wang, X.; Fang, X.; Liu, Y.; Zhao, P.; Cui, R. Modeling and control strategy analysis of a hydraulic energy-storage wave energy conversion system. *Renew. Energy* **2022**, *182*, 969–981. [CrossRef]
19. Zhu, T.; Xie, H.; Yang, H. Design and tracking control of an electro-hydrostatic actuator for a disc cutter re-placement manipulator. *Autom. Constr.* **2022**, *142*, 104480. [CrossRef]
20. Na, J.; Li, Y.; Huang, Y.; Gao, G.; Chen, Q. Output feedback control of uncertain hydraulic servo systems. *IEEE Trans. Ind. Electron.* **2020**, *67*, 490–500. [CrossRef]
21. Gao, B.; Shao, J.; Yang, X. A compound control strategy combining speed compensation with ADRC of electro-hydraulic position servo control system. *ISA Trans.* **2014**, *53*, 1910–1918. [CrossRef]
22. Yazdi, M.; Mohammadpour, J.; Li, H.; Huang, H.Z.; Zarei, E.; Pirbalouti, R.G.; Adumene, S. Fault tree analysis improvements: A bibliometric analysis and literature review. *Qual. Reliab. Eng. Int.* **2023**, *39*, 1639–1659. [CrossRef]
23. Zhang, J.; Shen, Y.; Gan, M.; Su, Q.; Lyu, F.; Xu, B.; Chen, Y. Multi-objective optimization of surface texture for the slipper/swash plate interface in eha pumps. *Front. Mech. Eng.* **2022**, *17*, 48–51. [CrossRef]
24. Nguyen, M.H.; Dao, H.V.; Ahn, K.K. Active disturbance rejection control for position tracking of electro-hydraulic servo systems under modeling uncertainty and external load. *Actuators* **2021**, *10*, 20. [CrossRef]
25. Du Phan, V.; Vo, C.P.; Dao, H.V.; Ahn, K.K. Robust fault-tolerant control of an electrohydraulic actuator with a novel nonlinear unknown input observer. *IEEE Access* **2021**, *9*, 30750–30760. [CrossRef]
26. Zad, H.S.; Ulasyar, A.; Zohaib, A. Robust Model Predictive position Control of direct drive electro-hydraulic servo system. In Proceedings of the 2016 International Conference on Intelligent Systems Engineering (ICISE), Islamabad, Pakistan, 15–17 January 2016. [CrossRef]
27. Ali, S.A.; Christen, A.; Begg, S.; Langlois, N. Continuous-Discrete Time-Observer Design for State and Disturbance Estimation of Electro-Hydraulic Actuator Systems. *IEEE Trans. Ind. Electron.* **2016**, *63*, 4314–4324. [CrossRef]
28. Kim, W.; Shin, D.; Won, D.; Chung, C.C. Disturbance-Observer-Based Position Tracking Controller in the Presence of Biased Sinusoidal Disturbance for Electrohydraulic Actuators. *IEEE Trans. Control. Syst. Technol.* **2013**, *21*, 2290–2298. [CrossRef]

29. Helian, B.; Yao, B.; Chen, Z.; Yang, C. Designing an Improved Controller for a Pump Direct Driven Electro-Hydraulic System Using a Nonlinear Flow Mapping. In Proceedings of the Symposium on Fluid Power and Motion Control, Longboat Key, FL, USA, 7–9 October 2019; pp. 1–7.
30. Peng, X.; Gong, G.; Liao, X.; Wu, W.; Wang, H.; Lou, H. Modeling and Model Identification of Micro-Displacement Control Hydraulic System. *Chin. J. Mech. Eng.* **2017**, *53*, 6. [CrossRef]
31. Wang, Y. Study on Control Strategies for MultiCylinder Collaborative System of Hydraulic Support Group. Ph.D. Thesis, China University of Mining and Technology, Xuzhou, China, 2021.
32. Jiao, Z.; Yao, J. *Nonlinear Control of Electro-Hydraulic Servo System*; Science Press: Beijing, China, 2016; pp. 100–102.